Electromagnetic metamaterials sensor for structural integrity of zirconia doped on rare earth coating on stainless steels

Adriana Savin[1], Mihail Liviu Craus[1,2], Rozina Steigmann[1], Vitalii Turchenko[2], Frantisek Novy[3], Janez Grum[4]
1 National Institute for Research and Development for Technical Physics, Iasi, Romania, asavin@phys-iasi.ro
2 Joint Institute for Nuclear Research, Dubna, Moscow, Russia,
3 University of Žilina, Žilina, Slovak Republic
4 University of Ljubljana, Ljubljana, Slovenia

Abstract

The paper proposes the use of a nondestructive electromagnetic method for evaluation of zirconia coating on AISI 316L, based an electromagnetic sensor with metamaterial lens. Metamaterials, namely Conical Swiss Roll, operated in radiofrequency range can serve as electromagnetic flux concentrators. Electromagnetic lens composing the sensors are designed based on Fourier optic principles and allows the enhancement of the spatial resolution of method in order to evaluate quality of surface/adhesion coating-support. Complementary methods such as Scanning Electron Microscopy and X ray diffraction are employed to study the samples taken into consideration.

1. Introduction

Thermal barrier coating (TBC) is used as thermal protective layer dedicated to metallic components in high temperature region, on engines and gas turbines, resulting to high component reliability and operating temperature, leading in higher efficiency [1]. TBC is a system that consists of a ceramic coating with or without Thermally Grown Oxide (TGO) deposited on a metal support. The weakest part of TBC is the substrate-ceramic interface, where fractures can appear under the action of thermal shock. Previous papers have been focused on behavior analysis of TGO as intermediary layer and later, on the improving of the surface of the top layer submitted to loadings during functioning. The optimization of the substrate surface topography is preferably based on a more complete characterization in order to achieve a reasonable balance between the level of induced delamination stresses, mechanical bonding as well as a minimization of the defect size. For characterization and monitoring of TBC failure, detection of their delamination, nondestructive evaluation (NDE) methods are used; most of these are based on optical principles including mid-infrared reflectance [2], luminescence spectroscopy [3] and elastic optical scattering [4]. These methods allow detection of TBC delamination and pre-spall condition. Zirconia (ZrO_2) based ceramics, are preferred due to their advanced mechanical properties [5]. Laminar structures of Yttria Stabilized Zirconia (YSZ) TBC layers deposited on stainless steels are typically porous and the pore size and character depends on the process parameters. A decreasing of global coating porosities is preferred; especially those opened at the surface, in order to reduce to minimum the permeability of coating to oxidation. ZrO_2 doped with rare earths oxides is considered a good TBC material [6] due of its low thermal conductivity (~2.0 $m^{-1}K^{-1}$ at 1100 ^{0} C), refractory,

chemical inertness, and compatible thermal expansion coefficient [5], with metallic support. ZrO stabilized in tetragonal phase, namely Tetragonal Zirconia Poly-crystal (TZP) have CeO_2 and Y_2O_3 [7] as stabilizers. The dimensions of crystallites are in the range of hundreds of nanometers, conferring a high resistance to breaking, YSZ present high resistance to thermal shocks and fatigue until 1150^0C [8]. Usually, three low-pressure polymorphic forms of zirconia [5] can be found: monoclinic state (stable below 1170 °C), $P2_1/c$; tetragonal phase, $P4_2/nmc$ (stable between 1170÷2370 °C) and the cubic, *Fm-3m* phase (above 2370 °C). Under external stress, as grinding or impact, transition from the tetragonal (t) to monoclinic (m) phase can appear at normal temperatures, being followed by 3-12% volume increase, causing compressive stress of YSZ coating [9]. The nanocomposites, in which nanometer - sized second phase particles are dispersed within a ceramic matrix and/or at grain boundaries, have shown significant improvements in strength and creep resistance, even at high temperatures, and assure an exciting future in different technological fields. Recent papers analyses the mechanism of coating degradation due interfacial damages, combination of microstructure evolutions linked to the roughness evolution, damage of metal–ceramic interface due of porosity, delamination initiated on the existent defects [10], splat boundaries, micro-cracks and pores can also be seen on the top surface of the coatings[11]. This paper present an electromagnetic (EM) method, using an EM sensor with metamaterials (MM) lenses, for evaluation of ZrO_2 coating-based ceramics properties as a function of addition of Y_2O_3 in the structure of the original ceramics (differentiating the areas with good/inferior coating quality) on stainless steels - AISI 316L and offering the first indication in order to analyze structural properties. The results were compared with alternative methods of characterization are involved as Scanning Electron Microscopy (SEM) and X-ray diffraction (XRD).

2. Theoretical principle of the electromagnetic method

The EM NDE is a well-known method for the quality evaluation of conductive pieces and structures with the aim of discontinuities detection cracks, inclusions, voids etc. MMs can provide an engineered response to EM radiation that is not available from the class of naturally occurring materials. The size of the structure is typically smaller than the free space wavelength of incoming EM waves. Depending on the frequency of the incident EM field, the type and geometrical shape MM may have a high relative magnetic permeability either positive or negative [12] and allow the EM waves amplification [13]. These properties strongly depend on the geometry of MMs more than on its composition [13],[14]. The EM sensor (send-receiver type) [14] has the principle scheme given in Figure 1a and its construction in Figure 1b.

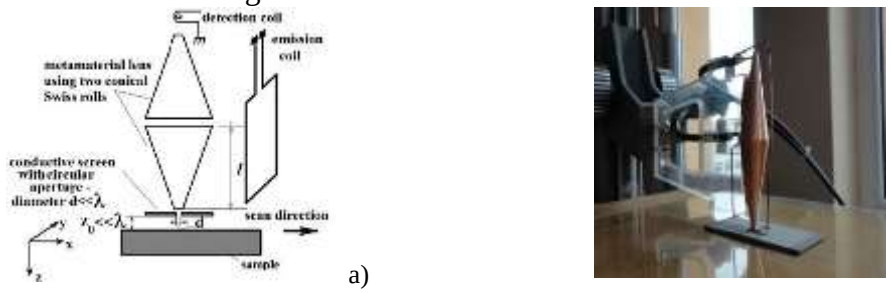

a) b)

Figure 1. Sensor with MM lens: a) principle scheme; b) physical realization

EM sensors with MM lens is made using Conical Swiss rolls (CSR) [14] the operation frequencies depending both by the constitutive parameters of MM lens as well as by the polarization of the incident EM field (transversal electric TE_z or transversal magnetic TM_z), in this case TM_z polarized at normal incidence. The emission part of the sensor is made from a single turn rectangular coil with 20x60mm^2 dimensions, placed at 25 mm distance from the lens [15]. The reception coil sensor has one turn with 1 mm average diameter placed in the focal image point, converting the localized energy into an electromotive force (e.m.f.).
Due to the radiofrequency flux concentration properties described in [14], the "ray" that pass inside traced, the plane "object" is in front of the aperture (figure 1a) and the focal plane is located in the plane of small base (where is placed detection coil).
Using Fourier optics [16], the field in focal plane of the lens is

$$H\left(x,y,z_0+2l\right)=\frac{H_0}{\pi^2}e^{j\left(\frac{k_b+k_a}{2}x+\frac{k_b+k_a}{2}y\right)}\frac{\sin\left(\frac{k_b-k_a}{2}x\right)}{x}\frac{\sin\left(\frac{k_b-k_a}{2}y\right)}{y} \quad (1)$$

when $z_0<<\lambda$, H_0 being the amplitude of incident magnetic field. In order to enhance spatial resolution, to ensure paraxial incident beam, in front of the sensor is placed a conductive screen having a circular aperture made from perfect electric conductive material with very small diameter. The diameter of focal spot of MM lens is [16]

$$D=\frac{4\pi}{\left(k_b-k_a\right)} \quad (2)$$

and it is equal with CSR small basis diameter i.e. 3.2 mm. When the lens is displaced along the scanning axis X, Figure 1a, k_a=0 and inserting in (2), k_b can be obtained and thus the field from (1). According to [17], on a relatively small distance, the field can be considered approximately constant. In this region, the reception device of the EM sensor with MM lens (with two CSRs tuned at 105MHz) is placed [15]. The scattered field must be also focused such that it can be detected by the reception part of the sensor placed in image focal point.

3. Studied samples

The AISI 316L steel (composition in wt. % as EN 1.4404) is susceptible to intergranular corrosion in certain corrosive media. TBC coating were deposited on samples (20x80mm^2 and 2 mm height) using plasma torch F400 with commercial atmospheric equipment APS 100 produced by Plasma-Technik AG. By doping with Yttria, a cation substitutive, supplementary oxygen vacancies are added to the molecular structure, increasing the ionic electrical conductivity. Pure yttrium oxide is a highly stable compound with a high melting point, is very inert chemically, and exhibits excellent electrical insulation (volume resistivity and dielectric breakdown strength).When Yttria is added to zirconia in concentration from 3% to 20% (molar percent), the crystalline structure of material in normal conditions is entirely stabilized [18], avoiding microcracking at temperature variation. Monolithic coatings consisting of various thickness zirconia doped with 3-20 % Y_2O_3 and sandwich zirconia doped with 20 % Y_2O_3 and Y_2O_3 coatings were deposited on AISI 316L[19]. The coating material is produced by Metco as powder Metco^{TM} 202NS and Metco 6035A. During the deposition, also samples without good adherence at support were obtained, being analyzed as well. For TBC the most important parameters are the thickness, thermal conductivity and density of coatings. In order to minimize the residual

stresses inside the sandwich coating-alloy support during the heating/cooling, the coating ZrO_2-Y_2O_3 shall be characterized.
The structure (cross sectional image of the sample deposited with ZrO_2 with 20 % Y_2O_3 with 0.2 mm respectivelly 20 % Y_2O_3 with 0.25 mm thick monolithic coating) is analyzed using Zeiss microscope in polarized light with Axio Imager A1m. Information about interface between support and zirconia coating are obtained by SEM and EDX. Taking into account that the structures of YSZ TBC layers deposited on stainless steels are typically porous, to obtain relevant information about the influence of Y_2O_3 concentration over the adherence at support, Secondary Electrons (SE) images, as well as Backscattered Electrons (BSE) images have been taken, Figure 2a and c. The information about porosity of coating is obtained by surface microscopy and soft gray scale threshold setting. The accuracy of gray scale threshold approach is investigated using image processing in Matlab described in [20]. In Figs. 2 b and d are presented the histograms of voids data.

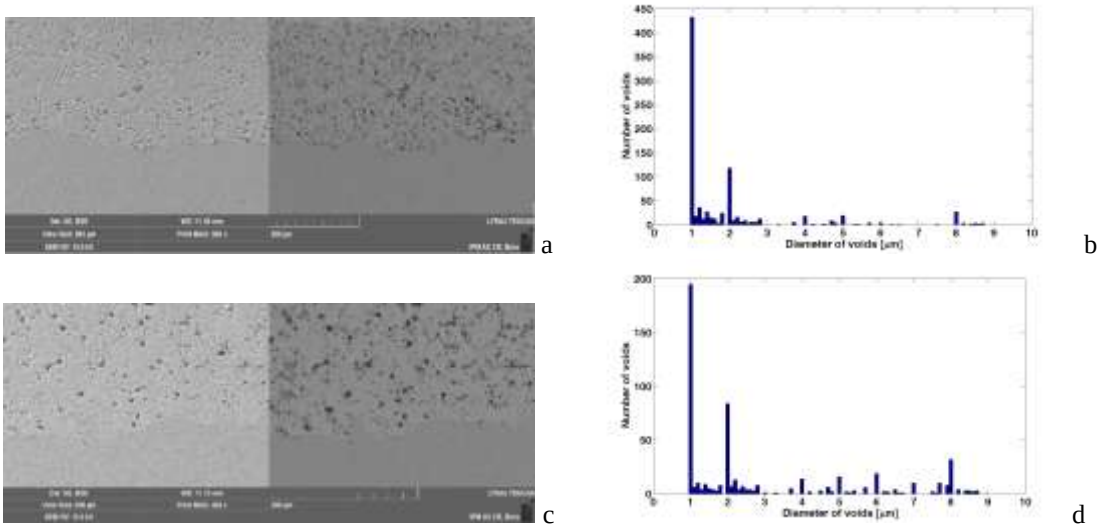

Figure 2. SEM images (left) and voids counting (right): a) and b) for specimen with 0.2 mm thin monolithic coating ZrO_2 with addition of 20 % Y_2O_3; c) and d) for specimen with sandwich coating 0.25 mm ZrO_2 with addition of 20 % Y_2O_3 and 0.005 mm Y_2O_3

It can be observed that with the doping with Y_2O_3, the voids are larger but their number decreases. Topographical characterization of the specimen is realized with a TESCAN electron microscope (TESCAN LYRA3 GM) operating at an acceleration voltage of 15 kV. The porosity of the tested surface can be evaluated from the SEM images within 0.5% accuracy. XRD experiments performed at room temperature on a Philips diffractometer, allow determination of the phase composition and microstructural parameters by using Fullprof software. The space group and lattice constants were obtained with Ceckcell and proofed by Fullprof software.
The comparisons between the diffractogram of the sample formed from a layer of zirconia doped with yttria deposited on a support of AISI316L with the diffractogram of AISI 316L and, respectively, with the diffractogram of zirconia doped with yttria allowed to identify austenite maxima (γ) (Figure 3a) and doped zirconia (t) maxima (Figure 3b).

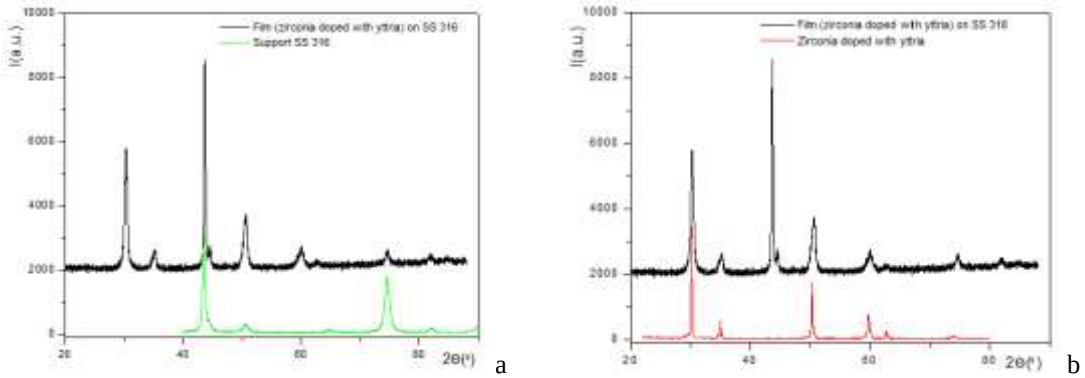

Figure 3. The Xray diffractograms: a) zirconia doped with yttria on support vs. support; b) zirconia doped with yttria on support vs. zirconia doped with yttria

4. Experimental setup of electromagnetic testing and results

ZrO_2-Y_2O_3 used as top-coating (is nonconductive and nonmagnetic) behaves like an air gap between conductive support and EM sensor, creating a lift-off for the EM sensor. The challenge for the development of new types of EM transducers consists in the obtaining of good detection sensitivity for a minimum 3/1 signal to noise ratio as well as a good spatial resolution.

As shown in [14], the sensor with a lens realized with CSR, functioning in the range of frequencies such that μ_{eff} is maximum. The detection principle is similar with the one of near-field electromagnetic scanning microscopy (NFESM). NFSEM imaging is a sampling technique, *i.e.*, the specimen (in this case plate with thickness of coating) is probed point by point by raster scanning with the sensor over the specimen surface and recording for energy image pixel a corresponding electromagnetic signature. Scattered EM field from other regions is eliminated by using MM lens with CSR with a conductive screen with circular aperture (made from perfect electric conductor material) the functioning of entire system detection can be described using Fourier optics [21]. The reception coil functions as a detection antenna, converting localized energy into emf. The electromagnetic NDE of a material consists in the applying a physical field to the object examined and evaluating the interaction between the field and the eventual material flaws. To increase the reliability and assure quality, an automatic scanning system is used, XY displacement system type Newmark together with a high frequency data acquisition [14]. The microstructure obtained by plasma jet can present lamellar or flattened splats with micro cracks through the splats or inter-splats. These splats lie parallel to the surface of the coating due to impact of the high-speed molten particles on the substrate.

The surface and bonding quality of support-layers are examined. The sensor with MM lens has allowed the identification and estimation of the zones where the nanoparticles have created shear distortions, possible to degenerate in the damage of the coatings. The samples were placed on the displacing system, with emission coil perpendicular on the surface and on scanning direction [15]. Ceramic zirconia top coating creates a probe lift-off effect. The specimens with 0.2 mm thickness of zirconia coating with and without yttria were fixed on a Newmark X-Y displacement system that assures the displacement in plane with ± 10 μm precision, for an lift-off of 75 μm. That enables scans of 5×5 mm^2 with 0.1 mm step in both directions, and the image delivered by the assembly sensor-equipment is amplified. Considering an object placed in the plane z = 0 and described by the function $f_0(x,y)$, at passing through an aperture, in the case of Fresnel diffraction (the

aperture is closely to the object), the image obtained at the distance *z* from the object will be $f_z(x,y)$ and can be calculated using the algorithm presented below according to the principle of Fourier optics

$$f_0(x,y) \rightarrow \boxed{\begin{matrix}2D \quad Fourier \\ Transform\end{matrix}} \xrightarrow{F_{(0)}(u,v)} \boxed{x\exp\left[-\frac{j2\pi^2}{k}\left(u^2+v^2\right)\right]} \xrightarrow{F_Z(u,v)} \boxed{\begin{matrix}Inverse \quad 2D \\ Fourier \quad Transform\end{matrix}} \rightarrow f_Z(x,y)$$

To ensure that $f_z(x,y)$ might represent exactly the figure of Fresnel diffraction through the a radius aperture, between the Fourier variables and the spatial ones must be

$$du = \frac{2a}{Ndx_0}; \quad dv = \frac{2a}{Mdy_0} \tag{4}$$

where N and M represent the maximum number of measurement points along x and y direction and dx_0 and dy_0 are the scanning step along x and respective y directions. Inverting the operation, the object $f_0(x,y)$ can be determined knowing the diffraction figure $f_z(x,y)$. The measurements effectuated with the aperture make that the signals recorded shall represents $f_z(x,y)$. The shape of the object that scatters the EM field created by the emission coil can be determined. Figures 4 a and b show the amplitude of the voltage induced in the reception coil of the EM transducer at the scanning of the two specimens presented above.

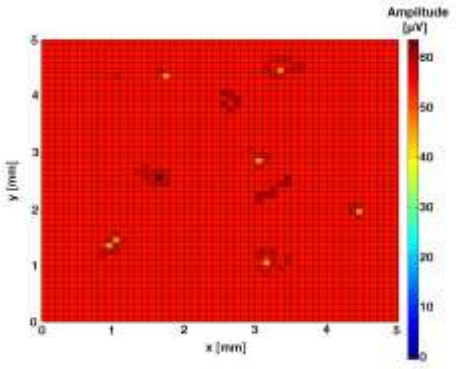

a

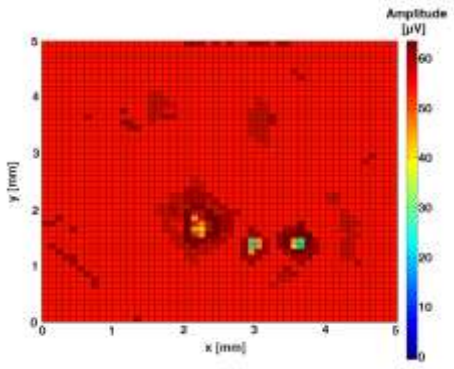

b

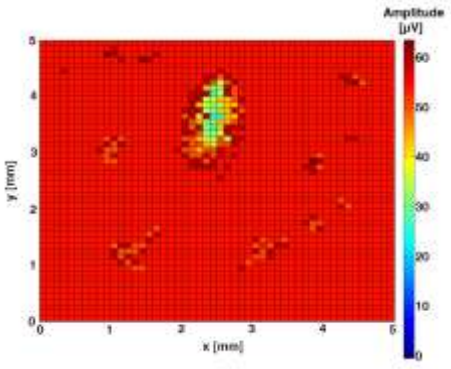

c

Figure 4 The amplitude of the voltage induced in the reception coil of the electromagnetic transducer: a) 0.2 mm thick monolithic coating ZrO_2 with addition of 20 % Y_2O_3; b) sandwich coating 0.25 mm ZrO_2 with addition of 20 % Y_2O_3 and 0.005 mm Y_2O_3; c) specimen with nonadherence from 0.25mm thick monolithic coating ZrO_2 with 20 % Y_2O_3 addition.

Figure 4 c presents the scanning of a specimen with no adherence from 0.25mm thick monolithic coating ZrO_2 with addition of 20 % Y_2O_3. It can be observed that the values of emf induced in the reception coils are affected by the material microstructure and by the presence of inhomogeneities on/in the surface of support. The image corresponding to 0.2 mm thick monolithic coating ZrO_2 with addition of 20 % Y_2O_3 do not present nonadherence regions. The amplitude of voltage induced in the reception coil has relatively constant value, excepting the regions where variations appear most probable due to agglomeration of oxides. Sandwich coatings 0.25 mm ZrO_2 with addition of 20 %Y_2O_3 and 0.005 mm Y_2O_3 show that at doping with yttria, the voids are more

extended but their number decreases, fact confirmed also by the SEM images.

It can be shown that the region with nonadherence is well emphasized. For specimens without adherence to support, the insular shape emphasized by the complementary methods is found on the representation of amplitude of voltage induced in the reception coil when the surface is scanned.

5. Conclusions

TBC potential depends not only by the intrinsic properties of TBC's material but of the coating microstructure that is determined by the deposition process. Nanocomposites with nanometer - sized second phase particles dispersed in ceramic matrix and/or at grain boundaries have shown an ability to withstand thermal cycling at temperatures significantly higher than simple layer YSZ-coatings. They also have significant better strength and creep resistance than other coatings. Hence the evaluation of the surface structure and possible delamination at the interface of deposited layers for this type of zirconia coating on stainless steel is important.

Using a MM lens, and following the method described above, from the zone inspected, the results allow the characterization of the surface microstructure and possible spallation/delamination at the interfaces of deposited layers. Also small roughness can be emphasized. The results of the NDT method have been confirmed by complementary methods. Further tests on a larger number of specimens with different coating aspects of the surface, influence of surface roughness on stress intensity factor, number of layers are needed to establish the accuracy of the results and the correlation between the located very small defect in size and the results of MM sensor response. Also, the results can be further continues by complementary investigation as neutron diffraction or other methods that can emphasize indications about phase composition and structure parameters.

Acknowledgements

This paper is supported by Ministry of Research and Innovation under Nucleus Program PN 2018 and Bilateral Cooperation with JINR Dubna protocol no. 04-4-1121-2015/2020.

References

1. U Schulz, C Leyens, K Fritscher, M Peters, B Saruhan-Brings, O Lavigne, JM Dorvaux, M Poulain, R Mévrel and M Caliez, "Some recent trends in research and technology of advanced thermal barrier coatings", Aerospace Science and Technology, 7(1), pp 73-80, 2003.
2. JL Eldridge, CM Spuckler, JA Nesbitt and KW Street, "Health monitoring of thermal barrier coatings by mid-infrared reflectance", NASA Technical report no. 20030022792, 2002
3. VK Tolpygo, DR Clarke and KS Murphy, "Evaluation of interface degradation during cyclic oxidation of EB-PVD thermal barrier coatings and correlation with TGO luminescence", Surface and Coatings Technology, 188, pp 62-70, 2004
4. WA Ellingson, RJ Visher, RS Lipanovich and CM Deemer, "Optical NDT techniques for ceramic thermal barrier coatings: NDT of ceramics: an introduction to the technical focus issue", Materials evaluation, 64(1), pp 45-51, 2006.
5. www.ceramtec.com, October 27, 2017

6. D Renusch and M Schütze, “Measuring and modeling the TBC damage kinetics by using acoustic emission analysis”, Surface and Coatings Technology, 202(4), pp 740-744, 2007.
7. WZ Zhu, “Effect of cubic phase on the kinetics of the isothermal tetragonal to monoclinic transformation in ZrO_2 (3mol% Y_2O_3) ceramics”, Ceramics International, 24, pp 35-43, 1998.
8. X Ren and W Pan, “Mechanical properties of high-temperature-degraded yttria-stabilized zirconia”, Acta Materialia, 69, pp 397-406, 2014.
9. V Lughi and DR Clarke, “High temperature aging of YSZ coatings and subsequent transformation at low temperature”, Surface and coatings technology, 200(5), pp 1287-1291, 2005.
10. AH Pakseresht, AH Javadi, E Ghasali, A Shahbazkhan and S Shakhesi, “Evaluation of hot corrosion behavior of plasma sprayed thermal barrier coatings with graded intermediate layer and double ceramic top layer”, Surface and Coatings Technology, 288, pp 36-45, 2016.
11. V Kumar and K Balasubramanian, “Progress update on failure mechanisms of advanced thermal barrier coatings: A review”, Progress in Organic Coatings, 90, pp 54-82, 2016.
12. JB Pendry, AJ Holden, DJ Robbins and WJ Stewart, “Magnetism from conductors and enhanced nonlinear phenomena”, IEEE transactions on microwave theory and techniques, 47(11), pp 2075-2084, 1999.
13. V Bladel, “Electromagnetic fields”, 2nded.; IEEE Press: Piscataway, NJ, USA, 2007.
14. R Grimberg, A Savin and R Steigmann, “Electromagnetic imaging using evanescent waves”, NDT & E International, 46, pp 70–76, 2012.
15. R Grimberg, A Savin, R Steigmann, B Serghiac and A Bruma, “Electromagnetic non-destructive evaluation using metamaterials”, INSIGHT, 53(3), pp 132-137, 2011
16. M Born and E Wolf, “Principles of Optics: Electromagnetic Theory of Propagation, Interference and Diffaction of Light”, Pergamon Press, Oxford, UK, 1959
17. R Grimberg, A Savin and J Rebello, “Electromagnetic Examination of Hydrogen Attack in AISI 4340 Steel”, Electromagnetic Nondestructive Evaluation (XVI), 38, pp 270, 2013.
18. C Pascual and P Duran, “Subsolidus Phase Equilibria and Ordering in the System ZrO2-Y2O3”, Journal of the American Ceramic Society, 66(1), pp 23-27, 1983
19. K Matsui, K Tanaka, T Yamakawa, M Uehara, N Enomoto and J Hojo, “Sintering kinetics at isothermal shrinkage: II, effect of Y_2O_3 concentration on the initial sintering stage of fine zirconia powder”, Journal of the American Ceramic Society, 90(2), p.443-447, 2007.
20. D Robinson, P Ramsundar and CB Samantaray, “Analyzing Porosity in Thermal Barrier Coatings: Edge Detection of Images using MATLAB”, 121st American Society of Engineering Education-ASEE Annual Conference, 2014.
21. JW Goodman and SC Gustafson, “Introduction to Fourier optics”, Optical Engineering, 35(5), pp1513-1513, 1996.